Turkish Computational and Theoretical Chemistry

Turkish Comp Theo Chem (TC&TC)

Volume(Issue): 9(5) – Year: 2025 – Pages: 26-39

e-ISSN: 2602-3237

https://doi.org/10.33435/tcandtc.1708544

Received: 28.04.2025 **Accepted:** 02.06.2025 *Research Article*

Activities of tetrahydrobenzothiazole derivative compounds against Nipah virus by HF method and Molecular docking calculations

Gamze Tüzün [1]

Department of Chemistry, Faculty of Science, Sivas Cumhuriyet University, Sivas, 58140, Turkey
Sivas, Turkey

Abstract: In this study, the electronic, biological and pharmacokinetic properties of eight tetrahydrobenzothiazole derivative molecules were investigated to evaluate their potential inhibitory activity against the Nipah virus. Quantum chemical calculations were performed at the HF/6-31++G(d,p) level using Gaussian 09 to determine parameters such as HOMO-LUMO energies, energy gap (ΔE), chemical hardness (η), softness (ε), electronegativity (χ), dipole moment, and total energy. Molecular docking simulations were conducted using the Schrödinger Maestro software against the viral proteins 2VSM and 4CO6, and their interactions were analyzed in terms of Glide scores, binding energies, and key molecular interactions. Additionally, ADME/T predictions were performed using the QikProp module to evaluate the drug-likeness and pharmacokinetic profiles of the compounds. The results showed that molecule 6 exhibited the highest stability and electrophilicity, while molecule 8 demonstrated the greatest reactivity and polarity. Molecule 3 was determined to have the most favorable ADME profile, including high permeability and oral absorption. These findings suggest that several of the studied compounds may serve as promising candidates for further antiviral drug development against the Nipah virus.

Keywords: Nipah virus, Molecular docking, DFT, Drug

1. Introduction

Nipah virus (NiV) is a negative-stranded, enveloped RNA virus that is zoonotic and causes high mortality in humans [1]. This virus, which belongs to the Henipavirus genus of the Paramyxoviridae family, was first identified in 1998 during an encephalitis outbreak in Malaysia that was transmitted to humans through contact with pigs [2]. Fruit bats belonging to the Pteropus genus have been identified as the viral reservoir, and transmission to humans occurs through direct contact with infected animals, contaminated foods (especially palm juice), or close human-to-human contact. Cases observed each year in endemic regions, especially in Bangladesh and India, show the continuity of the epidemic potential [3].

The clinical spectrum of NiV infection is wide, ranging from asymptomatic infection to acute respiratory disease and fatal encephalitis. The virus attaches to host cells, especially neurons and endothelial cells, through glycoproteins (G and F proteins) that have high affinity [4,5]. The G (attachment) glycoprotein binds to the ephrin-B2/B3 receptors on the host cell surface, allowing the virus to attach to the target cell. Then, the viral envelope and the host cell membrane fuse via the F (fusion) glycoprotein, and the genome is transferred to the cytoplasm. These two glycoproteins are of vital importance for the infectivity and tissue tropism of the virus and are therefore considered as the main target structures in modern vaccine development and inhibitor design studies.

Biochemically, the Nipah virus genome is approximately 18.2 kb long and encodes six structural proteins (N, P, M, F, G, L) [6]. Among these proteins, the N (nucleocapsid) protein stabilizes the RNA, while the L (large polymerase) and P (phosphoprotein) function in the replication

[1] Corresponding Authors

e-mail: gamzekekul@gmail.com

and transcription processes as part of the RNA-dependent RNA polymerase complex. The viral RNA undergoes replication in the host cell cytoplasm; this increases the sensitivity of the virus to cytoplasmic-targeted antiviral agents. In addition, various isoforms of the P protein (V, W and C proteins) suppress the interferon response and contribute to the virus's escape from the immune system [7].

When the chemical structure of the virus is examined, the three-dimensional structures of the G and F proteins are analyzed in detail with molecular docking and dynamic simulation techniques, and the binding energies of potential inhibitor compounds are calculated on these structures. Artificial intelligence-supported virtual screenings play an important role in the preliminary screening of drug candidates by evaluating the possible interactions of hundreds of thousands of small molecules with these proteins [8]. At the same time, the ADME/T (absorption, distribution, metabolism, excretion and toxicity) profiles of these compounds are analyzed with in silico methods, and their pharmacokinetic suitability is investigated [9]. New drug candidates are being developed against the Nipah virus with molecular modeling software such as Schrödinger Maestro, Autodock and HEX, which are used today.

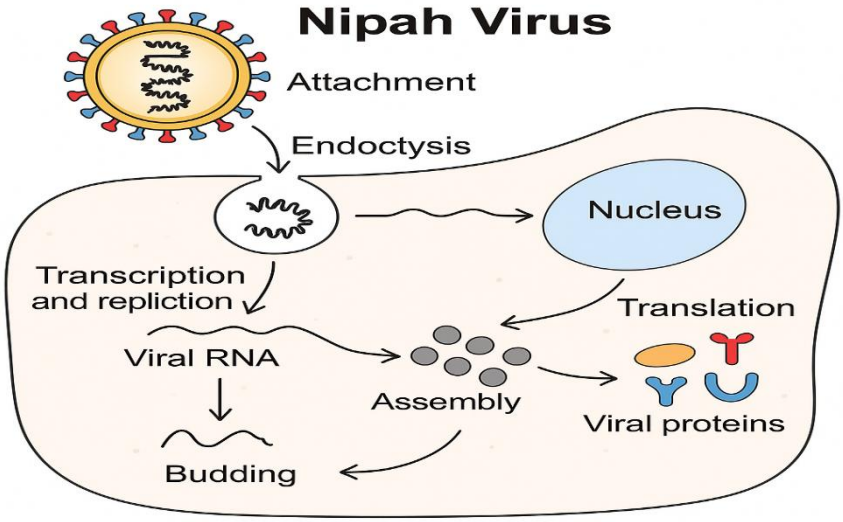

Figure 1. movement of nipah virus in cells

The high toxicity it shows on biological systems, cytokine storm, endothelial dysfunction and neuroinflammation-related complications make the pathophysiology of the virus more complex [10]. In this context, data obtained by molecular biology techniques are critical for elucidating genetic changes related to viral protein expression levels, immune response genes (e.g. interferons, IL-6, TNF-α) and apoptotic pathways. In addition, the pathological effects of NiV in human organoid models or animal models are guiding in the development of translational medicine [11].

The Nipah virus infection process begins with the virus binding to the host cell surface in Figure 1. At this stage, the virus attaches to receptors on the cell membrane via glycoproteins on its surface. After binding, the virus is taken into the cell via endocytosis [12]. The virus that enters the cell opens its capsid and releases its genome, that is, its viral RNA.

The released viral RNA undergoes replication in the cell cytoplasm using the host cell's mechanisms and multiplies through the transcription process [13]. The new RNAs obtained provide both new genome material and the templates necessary for the production of structural proteins.

The viral RNAs produced are processed in the cell's translation system and translated into various viral proteins [14]. These proteins are then brought together in the cytoplasm to provide assembly of new virus particles. The mature viruses formed as a result of this assembly process are budded from the cell membrane to the external environment and spread towards new cells to be infected [15]. This cycle causes the virus to multiply in the host and the infection to spread.

In this study, molecule 1 (S)-N1-(6-benzamido-4,5,6,7-tetrahydrobenzo[d]thiazol-2-yl)-N^8-Hydroxyoctanediamide, molecule 2 (S)-N1-(6-(4-fluorobenzamido)-4,5,6,7-tetrahydrobenzo[d] thiazol-2-yl)-N^8-hydroxyoctanediamide, molecule 3 (S)-N1-(6-(4-chlorobenzamido)-4,5,6,7-tetrahydrobenzo[d] thiazol-2-yl)-N^8-hydroxyoctanediamide, molecule 4 (S)-N1-(6-(4-bromobenzamido)-4,5,6,7-tetrahydrobenzo[d] thiazol-2-yl)-N8-hydroxyoctanediamide, molecule 5 (S)-N1-hydroxy-N^8-(6-(4-methylbenzamido)-4,5,6,7-tetrahydrobenzo[d]thiazol-2-yl)octanediamide, molecule 6 (S)-N1-hydroxy-N^8-(6-(4-methoxybenzamido)-4,5,6,7-tetrahydrobenzo[d]thiazol-2-yl)octanediamide, molecule 7 (S)-N1-(6-(furan-2-carboxamido)-4,5,6,7-tetrahydrobenzo[d] thiazol-2-yl)-N^8-hydroxyoctanediamide, molecule 8 (S)-N1-(6-(1-naphthamido)-4,5,6,7-tetrahydrobenzo[d]thiazol-2-yl)-N^8-hydroxyoctanediamide molecules were all synthesized by Sun and co-worker [16] in Figure 1. Then, the quantum chemical parameters of these molecules were calculated with the Gaussian package program. Calculations using the 6-31++g(d,p) basis set in the HF [17] techniques were performed using these programs. Then, the activities of the molecules against various proteins, which are PDB ID: 2VSM [18] and 4CO6 [19] proteins, were compared. Finally, the drug properties of the molecules were examined by ADME/T analysis of the molecules.

2. Computational Method

The chemical and biological properties of molecules can be significantly deduced from theoretical computations. Theoretical simulations yield extensive insights on quantum chemical parameters. The calculated parameters elucidate the chemical reactivity of the compounds. Molecules are computed utilizing several applications. Gaussian09 RevD.01 and GaussView 6.0 are the designations of these distinct apps [20,21]. Calculations employing the 6-31++g(d,p) basis set with the HF methods was conducted utilizing these programs. Numerous quantum chemical parameters have been identified by these quantum chemistry calculations. The subsequent presentation illustrates the calculated parameters, each representing a unique molecular chemical characteristic [22,23]. The equations for determining these parameters are shown in equations.

$$\chi = -\left(\frac{\partial \mathrm{E}}{\partial \mathrm{N}}\right)_{\upsilon(r)} = \frac{1}{2}(I + A) \cong \frac{1}{2}(E_{HOMO} + E_{LUMO})$$

$$\eta = -\left(\frac{\partial^2 \mathrm{E}}{\partial \mathrm{N}^2}\right)_{\upsilon(r)} = \frac{1}{2}(I - A) \cong -\frac{1}{2}(E_{HOMO} - E_{LUMO})$$

$$\sigma = 1/\eta \qquad \omega = \chi^2/2\eta \qquad \varepsilon = 1/\omega$$

Molecular docking calculations are employed to compare the biological activities of molecules with biological materials. Molecular docking computations were conducted utilizing Schrödinger's Maestro Molecular modeling platform (version 13.4) [24]. Calculations encompass multiple phases. Each phase is executed distinctly. Proteins were synthesized in the initial phase utilizing the protein preparation module [25]. The active sites of the proteins were found in this module. The subsequent phase entails the preparation of the compounds under investigation. The LigPrep module [26] is prepared for computations using optimized structures once the molecules have been initially optimized in the Gaussian software application. Subsequent to preparation, the interactions between the compounds and the cancer protein were examined utilizing the Glide ligand docking module [27,28]. All calculations were executed with the OPLS4 methodology. The pharmacological potential of the examined substances will be assessed using ADME/T study (absorption, distribution, metabolism, excretion, and toxicity). The impacts and responses of substances in human metabolism were forecasted utilizing the Qik-prop module of Schrödinger program [29].

3. Results and discussion

Understanding terminology such as the ΔE energy gap, E_{HOMO}, E_{LUMO}, chemical hardness, softness, electronegativity, and chemical potential is essential for grasping the electronic structure and chemical properties of molecules [30]. These are the essential criteria employed to assess the stability and reactivity of a chemical.

The energy gap, or ΔE, quantifies the difference in energy levels between a molecule's highest occupied molecular orbital (HOMO) and lowest unoccupied molecular orbital (LUMO) [31]. To completely understand the electrical stability and reactivity of a molecule, one must possess a comprehensive understanding of this value. A bigger ΔE value implies a more stable molecule structure, whereas a smaller ΔE value denotes heightened molecular reactivity [32].

In the realm of molecular orbital energy, E_{HOMO} and E_{LUMO} denote the energy of the highest occupied molecular orbital and the lowest unoccupied molecular orbital, respectively. The LUMO indicates a molecule's capacity to accept electrons, reflecting electrophilic behavior, whereas the HOMO governs a molecule's propensity to donate electrons, signifying nucleophilic activity [33]. Understanding the mechanics of electron transport in chemical processes necessitates a comprehensive grasp of the energy differential between the HOMO and LUMO states.

Chemical hardness refers to a molecule's capacity to endure alterations induced by external factors. More rigid molecules have reduced reactivity and enhanced structural stability. Chemical softness quantifies a molecule's reactivity; softer molecules exhibit greater susceptibility to alterations in their chemical structure. The concepts of softness and hardness may assist in predicting chemical bond formation and elucidating the acid-base properties of molecules [34].

Electronegativity is a crucial determinant of the polarity of chemical bonds. It is a phrase that denotes the tendency of an atom or molecule to attract bonding electrons. Compounds with elevated electronegativity are more effective at attracting electrons and exhibiting electrophilic characteristics in chemical processes.

Chemical potential quantifies the energy change within a molecule and indicates the system's response to fluctuations in electron density [31]. This value is a significant indicator in assessing molecular stability and reaction energy.

When integrated, these concepts establish a comprehensive basis for understanding the electrical structure, stability, and chemical reactivity of molecules. The assessment of HOMO and LUMO energy levels, in conjunction with ΔE, offers a valuable method for predicting chemical reactivity. Attributes such as electronegativity, malleability, and chemical hardness are crucial for comprehending molecular responses to external stimuli. All factors are comprehensively enumerated in Table 1 and Figure 2.

Table 1. The calculated quantum chemical parameters of molecules.

	E_{HOMO}	E_{LUMO}	I	A	ΔE	η	μ	χ	PA	ω	ε	dipol	Energy
HF/6-31++g(d,p) LEVEL													
1	-6.2249	-1.3617	6.2249	1.3617	4.8633	2.4316	0.4112	3.7933	-3.7933	2.9587	0.3380	4.2117	-40849.7670
2	-6.3509	-1.4283	6.3509	1.4283	4.9226	2.4613	0.4063	3.8896	-3.8896	3.0734	0.3254	4.6627	-38803.3891
3	-6.3479	-1.4169	6.3479	1.4169	4.9310	2.4655	0.4056	3.8824	-3.8824	3.0568	0.3271	4.6850	-40941.6618
4	-6.5117	-1.7454	6.5117	1.7454	4.7664	2.3832	0.4196	4.1285	-4.1285	3.5761	0.2796	3.6492	-50240.6179
5	-6.4970	-1.5867	6.4970	1.5867	4.9103	2.4552	0.4073	4.0419	-4.0419	3.3270	0.3006	3.6481	-40434.7499
6	-6.7898	-3.2042	6.7898	3.2042	3.5857	1.7928	0.5578	4.9970	-4.9970	6.9638	0.1436	5.3898	-43299.0681
7	-6.5237	-2.1704	6.5237	2.1704	4.3533	2.1767	0.4594	4.3471	-4.3471	4.3408	0.2304	5.2673	-45003.6194
8	-6.5683	-2.3987	6.5683	2.3987	4.1696	2.0848	0.4797	4.4835	-4.4835	4.8210	0.2074	5.7166	-41887.1637

Koopman's theorem [35], a basic principle in molecular orbital theory, correlates a molecule's electron affinity and ionization energy with its HOMO and LUMO energy levels. The hypothesis posits that the energy of the HOMO corresponds to the ionization energy of the molecule, whereas the energy of the LUMO reflects the electron affinity of the molecule. This approach provides a robust instrument for forecasting the electrical characteristics and reactivity of molecules. The findings are mere conjectures that may require more intricate computations for validation, given that the theory disregards electron-electron interactions.

The Hard and Soft Acid-Base (HSAB) paradigm [36] was developed to elucidate acid-base

chemistry. This perspective posits that hard acids have strong interactions with hard bases, whereas soft acids form robust connections with soft bases [37]. This theory posits that a system frequently assumes a structure with enhanced hardness due to its greater stability and reduced reactivity. This notion provides a valuable basis for forecasting the stability of molecules and chemical reactions. The concept of maximum hardness [38] is frequently employed, especially in evaluating transition states and generating reactive intermediates.

These three fundamental concepts offer a theoretical and practical foundation for a thorough comprehension of the properties of molecular bonding and reactivity. The HSAB principle elucidates the characteristics of acid-base interfaces [39], Koopman's theorem examines electron transport pathways, and PMH predominantly forecasts molecular stability [40]. The integration of these methodologies may yield a comprehensive understanding of chemical system behavior.

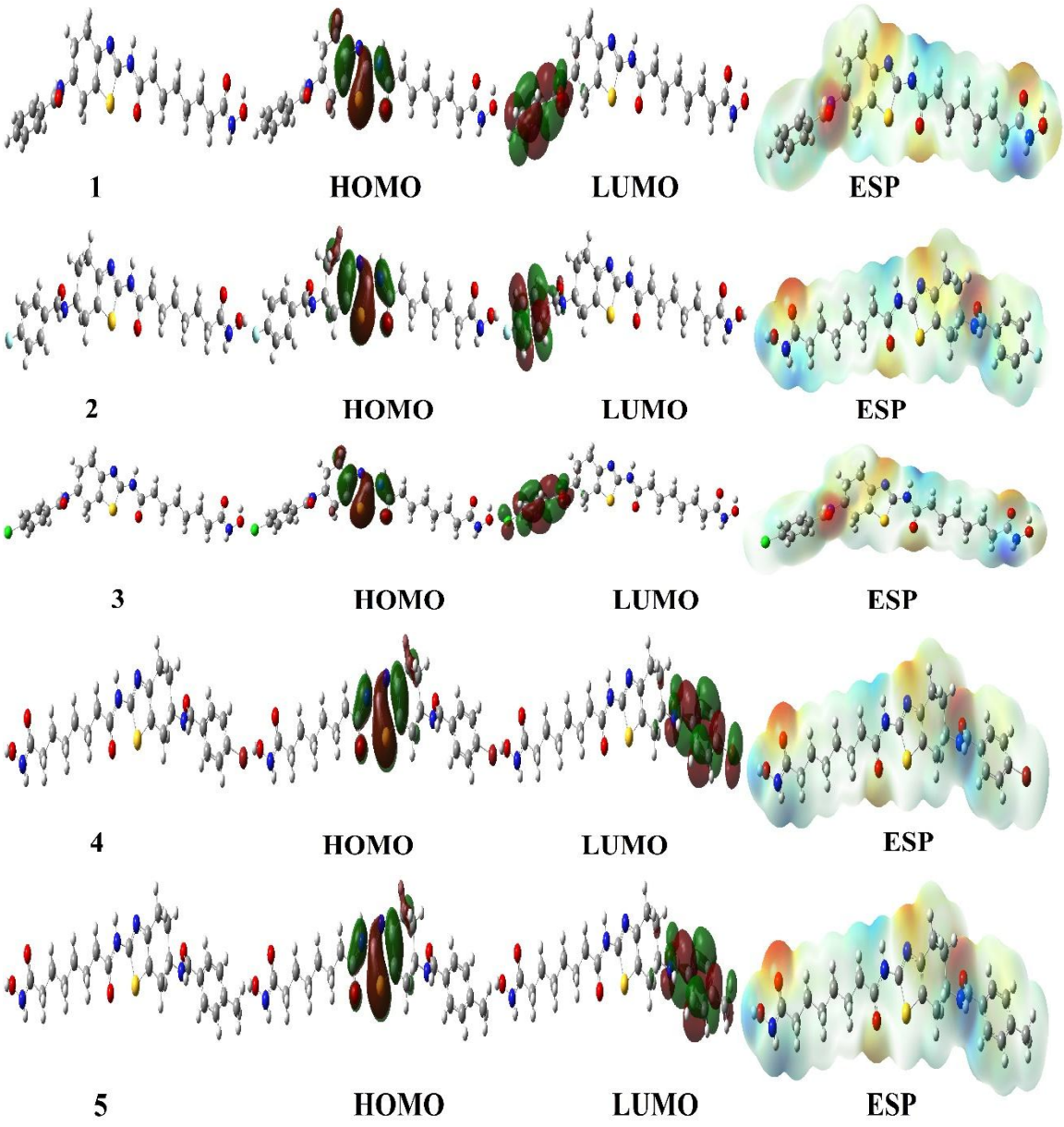

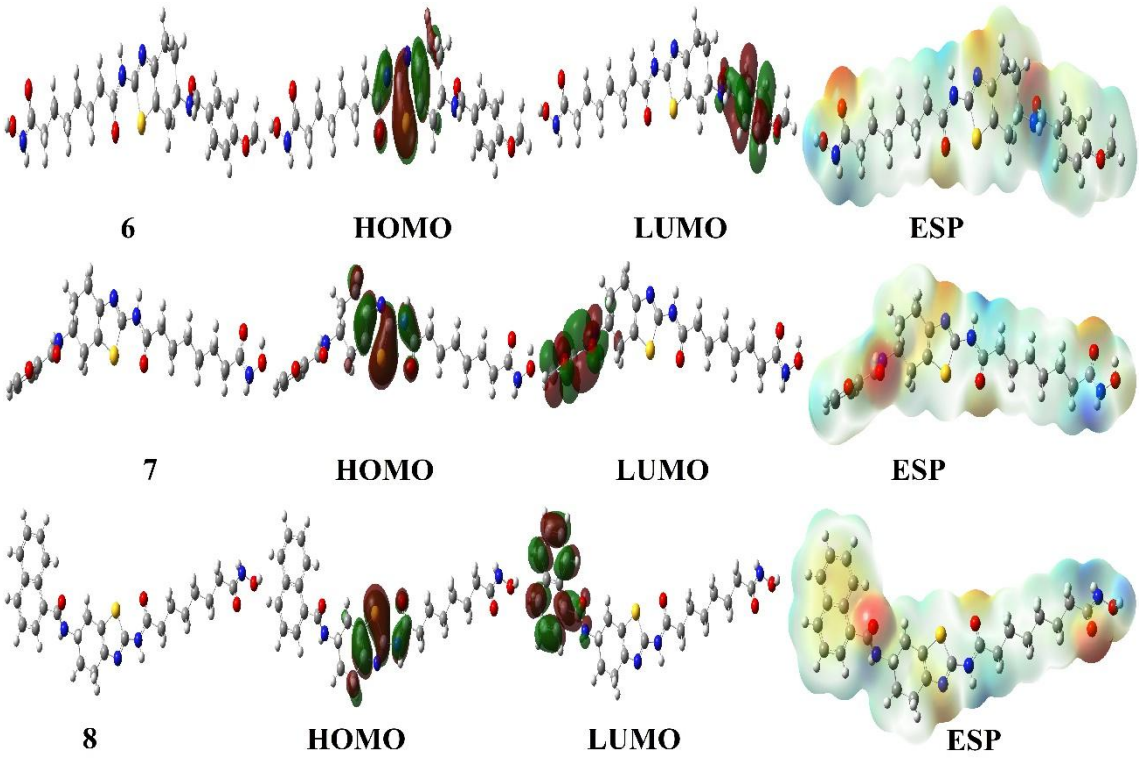

Figure 2. Representations of optimize structure, HOMO, LUMO, and ESP of molecules

As a result of the Hartree-Fock calculations, many quantum chemical parameters of the molecules were calculated. The HOMO-LUMO energy range (ΔE) provides information about the chemical reactivity and stability of the molecules. Molecules with low ΔE values are considered more reactive, while those with high values are considered more stable. In this context, the molecule with the lowest ΔE value is 8 (4.1696 eV) and this molecule stands out as the most reactive structure. The highest ΔE value was observed in molecule 6 (6.7898 eV) and it was understood that this molecule has the most stable structure.

Chemical hardness (η) values are calculated as half of ΔE and show the resistance of the molecules to external factors. The highest hardness value was calculated in molecule 6, and the lowest value was calculated in molecule 8. In contrast, chemical softness (ε) shows the flexibility and reactivity of the molecules; According to this parameter, the softest molecule is 8.

The electrophilicity index (ω) indicates the electrophilic character of a molecule. A high value indicates that the molecule has a high ability to interact with nucleophiles. When evaluated from this perspective, molecule 6 has the highest electrophilicity index (6.963), showing a strong electrophilic character. The lowest electrophilicity value was found in molecule 8 (4.821), showing that it is less prone to electrophilic reactions.

Dipole moment values indicate the polarity of molecules. The highest dipole moment is shown in molecule 8 (5.7166 Debye), showing that it can interact more with polar solvents. In contrast, the lowest dipole moment was calculated in molecule 1 (4.2117 Debye), showing that this structure exhibits a more nonpolar character.

Finally, the total energy values show the thermodynamic stability of the molecules. The lowest (i.e. most stable) total energy value was calculated for molecule 4 (–50240.6179 eV), which shows that it may be the most stable structure. The molecule with the highest energy is molecule 2 (–38803.3891 eV), and this structure is less stable compared to the others. When evaluated in general, molecule 6 stands out with its high stability and electrophilicity properties, while molecule 8 draws attention with its reactivity, softness and high polarity. Molecule 4 was determined as the most stable structure in terms of total energy. These findings show that the electronic properties of the molecules change significantly depending on the

structural differences and are guiding for future experimental studies.

Table 2. Numerical values of the docking parameters of molecule against protein

2VSM	Docking Score	Glide ligand efficiency	Glide hbond	Glide evdw	Glide ecoul	Glide emodel	Glide energy	Glide einternal	Glide posenum
1	-6.23	-0.20	-0.29	-47.08	-13.51	-78.19	-60.59	7.77	319
2	-6.04	-0.19	-0.42	-44.14	-10.96	-71.99	-55.10	5.32	160
3	-6.69	-0.21	0.00	-53.27	-8.74	-74.64	-62.01	20.65	169
4	-6.51	-0.20	-0.84	-46.60	-10.13	-73.64	-56.73	6.54	388
5	-5.66	-0.18	-0.02	-59.30	-1.82	-53.33	-61.12	30.48	124
6	-5.88	-0.18	-0.72	-47.98	-6.78	-70.94	-54.76	8.41	254
7	-6.57	-0.23	-0.85	-38.59	-9.44	-66.38	-48.03	9.33	243
8	-4.55	-0.13	-0.30	-51.93	-6.48	-41.32	-58.41	28.28	83
4CO6	Docking Score	Glide ligand efficiency	Glide hbond	Glide evdw	Glide ecoul	Glide emodel	Glide energy	Glide einternal	Glide posenum
1	-6.23	-0.20	-1.41	-29.46	-21.26	-68.88	-50.72	8.84	229
2	-6.40	-0.20	-1.10	-33.05	-19.77	-70.05	-52.81	11.04	343
3	-6.28	-0.20	-1.56	-31.53	-20.45	-70.71	-51.98	8.11	75
4	-5.64	-0.18	-1.43	-33.34	-18.89	-66.43	-52.24	8.71	227
5	-6.35	-0.20	-1.38	-32.05	-21.59	-72.63	-53.65	7.12	242
6	-6.32	-0.19	-1.36	-32.11	-20.25	-69.93	-52.37	10.40	350
7	-5.58	-0.19	-1.37	-29.59	-19.39	-62.89	-48.98	11.00	392
8	-6.02	-0.17	-1.37	-32.01	-19.98	-67.48	-51.98	12.79	149

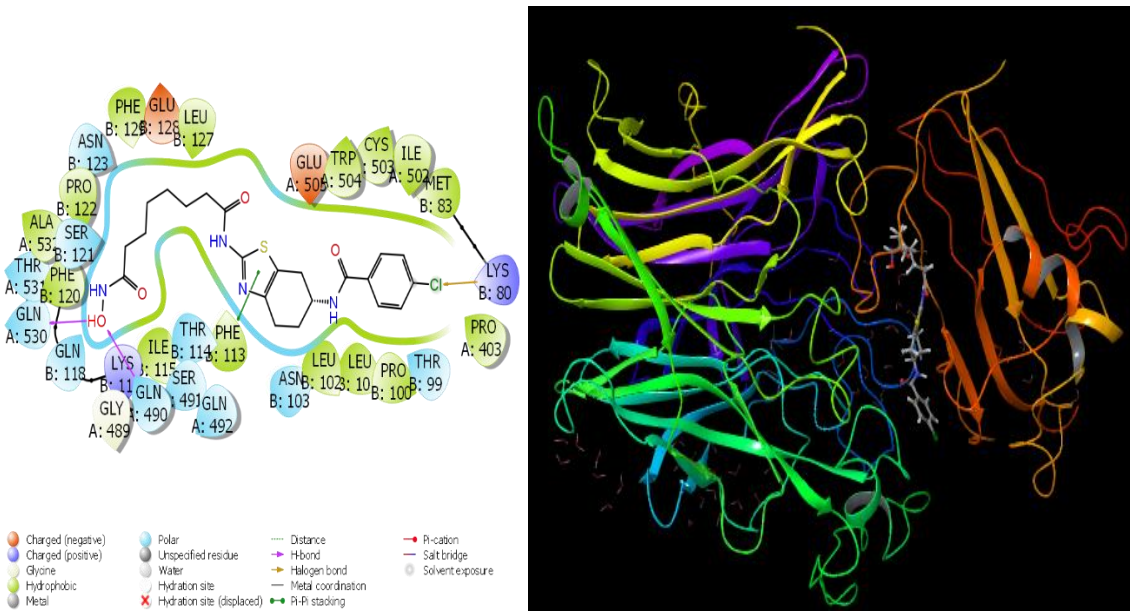

Figure 3. Presentation interactions of molecule 3 with 2VSM protein

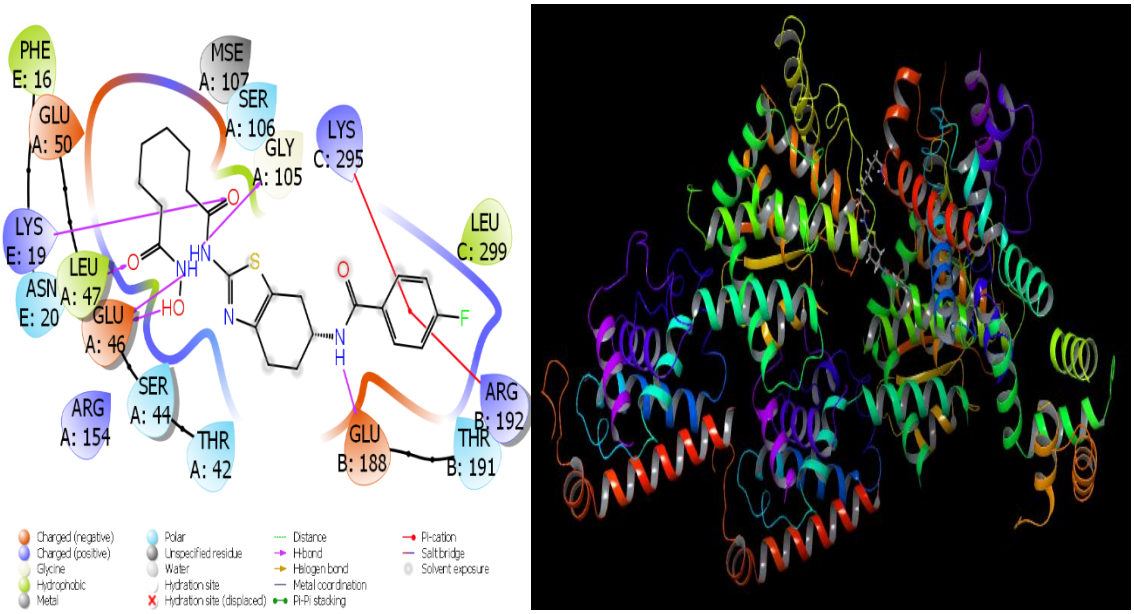

Figure 4. Presentation interactions of molecule 2 with 4CO6 protein

Recent research indicates that the comparison of the biological activities of molecules has been significantly accelerated and made simpler as a result of the extensive use of theoretical research and technological breakthroughs [41]. These two research methodologies have been utilized extensively, which has led to this being the result. The findings of the most recent research lend credence to this assertion. Calculations have significantly sped up and simplified the process of determining which medications are the most effective and successful prior to the testing of those medications in experimental settings [42]. There were a number of factors that were revealed by the theoretical computations. In order to determine the nature of the connection that exists between the numerical values of these parameters and the functioning of molecules in biological systems, this method is utilized. In order to accurately evaluate the biological parameters, this is carried out. The interactions that take place between different proteins and chemicals are the most important factor that has an effect on the activities that have been described there [43]. The proteins are ultimately inhibited as a result of the widely distributed nature of these interactions. The inhibition process takes place through this particular mechanism. The energy levels of proteins are determined by the way in which chemicals interact with that protein. Hydrogen bonds, polar and hydrophobic contacts, π-π interactions, and halogen interactions are the various ways in which molecules and proteins interact with one another [44-46]. Interaction between molecules is essential for maintaining equilibrium at a constant level. Numerous in-depth investigations into these chemical interactions have revealed that there are a great deal of distinct ways in which proteins and chemicals interact with one another. On the other hand, all of the figures can be found in Figures 3 and 4, and Table 2 contains all of the characteristics. In molecular docking simulations, the most important parameter that is derived is the Glide ligand efficiency calculation. These are not the only characteristics that complement one another. An illustration of how effectively the ligand works

against specific bacterial proteins is provided by this numerical chart. It is possible to determine the amount of hydrogen bonds that are formed as a result of interactions between molecules and proteins by using the Glide Hbond [47]. Among the statistics that illustrate the ways in which chemicals and proteins interact with one another is the Van der Waals interaction number, which is also commonly referred to as Glide Evdw [48]. Furthermore, in order to conduct an objective evaluation of the Coulomb interactions that take place between drugs and proteins, a metric known as Glide Ecoul is utilized. The final parameter that is reached as a result of these computations is the Glide Einternal, which is a numerical value that is obtained by integrating a large number of components [49].

Table 3. ADME properties of molecule

	1	**2**	**3**	**4**	**5**	**6**	**7**	**8**	**Referance Range**
mol_MW	445	463	479	523	459	475	439	495	130-725
dipole (D)	8.5	6.4	6.4	4.3	6.5	4.9	7.0	6.9	1.0-12.5
SASA	817	824	842	856	858	856	888	877	300-1000
FOSA	331	330	331	325	413	414	490	329	0-750
FISA	239	238	239	255	255	255	284	240	7-330
PISA	205	167	157	158	150	147	76	272	0-450
WPSA	43	89	115	119	41	41	39	37	0-175
volume (A^3)	1422	1436	1468	1495	1502	1513	1497	1556	500-2000
donorHB	4	4	4	4	4	4	4.333	4	0-6
accptHB	10.7	10.7	10.7	10.7	10.7	11.4	11.0	10.7	2.0-20.0
glob (Sphere =1)	0.7	0.7	0.7	0.7	0.7	0.7	0.7	0.7	0.75-0.95
QPpolrz (A^3)	45.6	45.9	47.0	48.1	48.3	48.1	46.1	51.7	13.0-70.0
QPlogPC16	16.1	15.7	16.8	17.2	16.7	16.7	16.7	17.9	4.0-18.0
QPlogPoct	27.6	27.6	28.1	28.3	28.2	28.4	28.0	29.5	8.0-35.0
QPlogPw	21.1	20.9	20.9	21.1	21.0	21.5	21.1	21.7	4.0-45.0
QPlogPo/w	1.4	1.7	1.9	2.0	1.7	1.5	1.2	2.3	-2.0-6.5
QPlogS	-4.4	-4.7	-5.1	-5.3	-5.0	-4.6	-5.1	-5.4	-6.5-0.5
CIQPlogS	-3.9	-4.2	-4.6	-5.4	-4.2	-4.2	-3.3	-5.1	-6.5-0.5
QPlogHERG	-5.2	-5.0	-5.1	-5.1	-5.1	-5.0	-5.2	-5.7	*
QPPCaco (nm/sec)	29	30	29	21	21	21	11	29	**
QPlogBB	-2.8	-2.7	-2.7	-2.9	-3.1	-3.1	-3.9	-2.9	-3.0-1.2
QPPMDCK (nm/sec)	36	66	89	64	24	24	12	32	**
QPlogKp	-4.1	-4.3	-4.3	-4.6	-4.6	-4.5	-5.2	-3.9	Kp in cm/hr
IP (ev)	9.1	9.2	9.2	9.6	9.6	9.6	8.2	8.9	7.9-10.5
EA (eV)	0.9	1.1	1.1	0.9	0.8	0.8	1.1	1.1	-0.9-1.7
#metab	5	5	5	5	6	6	5	5	1-8
QPlogKhsa	-0.5	-0.5	-0.4	-0.3	-0.3	-0.5	-0.5	-0.2	-1.5-1.5
Human Oral Absorption	2	2	2	2	2	2	2	2	-
Percent Human Oral Absorption	62	63	65	49	61	59	40	66	***
PSA	149	149	149	158	158	168	174	154	7-200
RuleOfFive	0	0	0	1	0	0	1	0	Maximum is 4
RuleOfThree	0	0	0	1	1	1	1	0	Maximum is 3
Jm	0.0	0.0	0.0	0.0	0.0	0.0	0.0	0.0	-

ADME/T parameters of eight molecules evaluated in this study were calculated using the Schrödinger QikProp module, are given in Table 3. These parameters enable the pharmacokinetic investigation of drug-like properties and the prediction of the behavior of molecules in biological systems [50].

Molecular weight (mol_MW) values range from 445 to 523 g/mol, which is within the reference range of 130–725 g/mol. This indicates that the molecules comply with Lipinski's rules and have the characteristics of being potential drug candidates. The dipole moments of the molecules range from 4.3 to 8.5 Debye, which are considered

appropriate in terms of polarity, and molecule 1 stands out with its high polarity [51,52].

Total surface area (SASA) values are in the range of 817–888 Å², and these values are within acceptable limits in terms of biological membrane permeability. When the hydrophobic (FOSA), hydrophilic (FISA), positive (PISA) and total polar (WPSA) surface area data are evaluated, it is seen that the surface area distributions of the molecules are balanced and that they have a structure that can interact with biological systems. The molecule with the highest hydrophilic surface area is 7 (FISA: 284). The volume values of the molecules are between 1422–1556 Å³, which is in line with the recommended range for drug-like molecules [53,54].

The hydrogen bond donation (donorHB) and acceptance (accptHB) capacities vary between approximately 4 and 10.7–11.4, respectively, and these values indicate the interaction capabilities of the molecules with aqueous environments. All molecules have suitable properties in this respect. The sphericity parameter (Glob) was calculated as 0.7 for all molecules, and although it is slightly below the ideal value (0.75–0.95), this value is tolerable for complex molecules [55].

When examined in terms of pharmacokinetic parameters, QPPCaco values simulating the passage through the Caco-2 cell membrane were calculated as the highest for molecule 3 (89 nm/s) and it was seen that this molecule was advantageous in terms of gastrointestinal absorption. Other molecules, especially molecule 7, showed low permeability (11 nm/s) and this indicated that the molecule in question may be weaker in terms of oral bioavailability. QPPMDCK values indicating passage through the MDCK cell membrane were similarly calculated as the highest for molecule 3 (89 nm/s). QPlogBB values representing brain-blood barrier passage were between -2.7 and -3.9 for all molecules, indicating that these molecules have a low potential to reach the central nervous system. QPlogKp values expressing skin penetration ranged between -3.9 and -5.2 and these values were low in terms of skin absorption. The human oral absorption rate (Human Oral Absorption) was determined as 2 for all molecules, indicating moderate absorption. When the percentage oral absorption values are examined, the highest absorption was observed in molecule 8 (66%), while the lowest was calculated in molecule 7 (40%) [56,57].

When examined toxicologically, QPlogHERG values indicating HERG channel inhibition potential vary between –5.0 and –5.7. These values are within safe limits in terms of cardiotoxicity and show that the molecules are reliable in terms of possible side effects. The solubility parameters QPlogS and CIQPlogS values vary between –3.3 and –5.4, indicating moderate water solubility [51,52,58].

When evaluated according to Lipinski's "Rule of Five" [59,60] and "Rule of Three" rules [61], most molecules comply with these rules and only minimal violations are observed for some molecules. Total polar surface area (PSA) values are in the range of 149–174 Å², and molecule 7 and molecule 6 have the highest PSA. These values are approaching the upper limits in terms of bioavailability, but are still at an acceptable level.

When evaluated in general, molecule 3 stands out as the compound with the best ADME profile with high gastrointestinal permeability, appropriate solubility and high oral absorption rate. Molecule 8 has the highest oral absorption rate, while molecule 7 has a weaker profile in this respect with low permeability and low absorption rate. All molecules have drug-like properties and comply with the Lipinski criteria. These results show that the compounds are promising in terms of bioavailability and drug potential.

4. Conclusions

The present study provides a comprehensive theoretical investigation of eight tetrahydrobenzothiazole derivatives in the context of potential antiviral activity against the Nipah virus. The quantum chemical descriptors calculated at the HF/6-31++G(d,p) level revealed significant variations in electronic properties among the compounds, with molecule 8 showing the highest reactivity and molecule 6 exhibiting the greatest electronic stability. Molecular docking studies demonstrated that several molecules exhibited strong interactions with target viral proteins, particularly molecule 3, which showed favorable docking scores and binding efficiency. ADME/T analysis further supported the drug-likeness of these molecules, highlighting molecule 3 as the most pharmacokinetically suitable candidate.

Collectively, the combination of quantum chemical, docking, and ADME data suggests that these compounds, particularly molecules 3, 6, and 8, represent promising leads for the design and development of novel inhibitors targeting the Nipah virus. Future experimental validation is recommended to confirm their therapeutic potential.

ACKNOWLEDGEMENT

The numerical calculations reported in this paper were fully/partially performed at TUBITAK ULAKBIM, High Performance and Grid Computing Center (TRUBA resources). This work was supported by the Scientific Research Project Fund of Sivas Cumhuriyet University (CUBAP) under the project number RGD-020.

References

[1] Ang, B. S., Lim, T. C., & Wang, L. Nipah virus infection. Journal of Clinical Microbiology, 56(6) (2018), 10-1128.

[2] Chua, K. B. Nipah virus outbreak in Malaysia. Journal of Clinical Virology, 26(3) (2003), 265-275.

[3] Harcourt, B. H., Lowe, L., Tamin, A., Liu, X., Bankamp, B., Bowden, N., ... & Rota, P. A. Genetic characterization of Nipah virus, Bangladesh, 2004. Emerging Infectious Diseases, 11(10) (2005), 1594.

[4] Li, Y., Liu, D., Wang, Y., Su, W., Liu, G., & Dong, W. The importance of glycans of viral and host proteins in enveloped virus infection. Frontiers in Immunology, 12 (2021), 638573.

[5] Choppin, P. W., & Scheid, A. The role of viral glycoproteins in adsorption, penetration, and pathogenicity of viruses. Reviews of Infectious Diseases, 2(1) (1980), 40-61.

[6] Sun, B., Jia, L., Liang, B., Chen, Q., & Liu, D. Phylogeography, transmission, and viral proteins of Nipah virus. Virologica Sinica, 33(5) (2018), 385-393.

[7] Sharma, V., Kaushik, S., Kumar, R., Yadav, J. P., & Kaushik, S. Emerging trends of Nipah virus: A review. Reviews in Medical Virology, 29(1) (2019), e2010.

[8] Harcourt, B. H., Tamin, A., Halpin, K., Ksiazek, T. G., Rollin, P. E., Bellini, W. J., & Rota, P. A. Molecular characterization of the polymerase gene and genomic termini of Nipah virus. Virology, 287(1) (2001), 192-201.

[9] Yalazan, H., Koç, D., Kose, F. A., Akgül, M. İ., Fandaklı, S., Tüzün, B., ... & Kantekin, H. Chalcone-based schiff bases: Design, synthesis, structural characterization and biological effects. Journal of Molecular Structure, 1337 (2025), 142211.

[10] Hsu, V. P., Hossain, M. J., Parashar, U. D., Ali, M. M., Ksiazek, T. G., Kuzmin, I., ... & Breiman, R. F. Nipah virus encephalitis reemergence, Bangladesh. Emerging Infectious Diseases, 10(12) (2004), 2082.

[11] Hughes, J. M., Wilson, M. E., Luby, S. P., Gurley, E. S., & Hossain, M. J. Transmission of human infection with Nipah virus. Clinical Infectious Diseases, 49(11) (2009), 1743-1748.

[12] Luby, S. P., Rahman, M., Hossain, M. J., Blum, L. S., Husain, M. M., Gurley, E., ... & Ksiazek, T. G. Foodborne transmission of Nipah virus, Bangladesh. Emerging Infectious Diseases, 12(12) (2006), 1888.

[13] Bonaparte, M. I., Dimitrov, A. S., Bossart, K. N., Crameri, G., Mungall, B. A., Bishop, K. A., ... & Broder, C. C. Ephrin-B2 ligand is a functional receptor for Hendra virus and Nipah virus. Proceedings of the National Academy of Sciences, 102(30) (2005), 10652-10657.

[14] Chua, K. B., Koh, C. L., Hooi, P. S., Wee, K. F., Khong, J. H., Chua, B. H., ... & Lam, S. K. Isolation of Nipah virus from Malaysian Island flying-foxes. Microbes and Infection, 4(2) (2002), 145-151.

[15] Chua, K. B., Bellini, W. J., Rota, P. A., Harcourt, B. H., Tamin, A., Lam, S. K., ... & Mahy, B. W. J. Nipah virus: a recently emergent deadly paramyxovirus. Science, 288(5470) (2000), 1432-1435.

[16] Sun, S., Zhao, W., Li, Y., Chi, Z., Fang, X., Wang, Q., ... & Luan, Y. Design, synthesis and antitumor activity evaluation of novel HDAC inhibitors with tetrahydrobenzothiazole as the skeleton. Bioorganic Chemistry, 108 (2021), 104652.

[17] Vautherin, D., & Brink, D. T. Hartree-Fock calculations with Skyrme's interaction. I. Spherical nuclei. Physical Review C, 5(3) (1972), 626.

[18] Bowden, T. A., Aricescu, A. R., Gilbert, R. J., Grimes, J. M., Jones, E. Y., & Stuart, D. I. Structural basis of Nipah and Hendra virus attachment to their cell-surface receptor ephrin-B2. Nature Structural & Molecular Biology, 15(6) (2008), 567-572.

[19] Yabukarski, F., Lawrence, P., Tarbouriech, N., Bourhis, J. M., Delaforge, E., Jensen, M. R., ... & Jamin, M. Structure of Nipah virus unassembled nucleoprotein in complex with its viral chaperone. Nature Structural & Molecular Biology, 21(9) (2014), 754-759.

[20] Dennington, R., Keith, T. A., & Millam, J. M. GaussView 6.0. Semichem Inc., Shawnee Mission, KS, USA, (2016).

[21] Frisch, M. J., Trucks, G. W., Schlegel, H. B., Scuseria, G. R., Robb, M. A., Cheeseman, J. R., ... & Fox, D. J. Gaussian 09, Revision D.01. Gaussian Inc., Wallingford, CT, USA, (2009).

[22] Allah, A. E. M. A., Mortada, S., Tüzün, B., Guerrab, W., Qostal, M., Mague, J. T., ... & Ramli, Y. Novel thiohydantoin derivatives: design, synthesis, spectroscopic characterization, crystal structure, SAR, DFT, molecular docking, pharmacological and toxicological activities. Journal of Molecular Structure, 1335 (2025), 141995.

[23] Dahmani, M., Titi, A., Kadri, S., ET-Touhami, A., Yahyi, A., Tüzün, B., ... & Warad, I. Synthesis of two new Sn (IV) carboxylate complexes: Crystal structures, density functional theory and Hirshfeld surface analysis computation, antibacterial, antifungal, and bioinformatics potential determination. Inorganic Chemistry Communications, (2025), 114683.

[24] Schrödinger Release 2022-4: Maestro. Schrödinger, LLC, New York, NY, USA, (2022).

[25] Schrödinger Release 2022-4: Protein Preparation Wizard; Epik; Impact; Prime. Schrödinger, LLC, New York, NY, USA, (2022).

[26] Schrödinger Release 2022-4: LigPrep. Schrödinger, LLC, New York, NY, USA, (2022).

[27] Shahzadi, I., Zahoor, A. F., Tüzün, B., Mansha, A., Anjum, M. N., Rasul, A., ... & Mojzych, M. Repositioning of acefylline as anti-cancer drug: Synthesis, anticancer and computational studies of azomethines derived from acefylline tethered 4-amino-3-mercapto-1,2,4-triazole. PLOS ONE, 17(12) (2022), e0278027.

[28] El Faydy, M., Lakhrissi, L., Dahaieh, N., Ounine, K., Tüzün, B., Chahboun, N., ... & Zarrouk, A. Synthesis, Biological Properties, and Molecular Docking Study of Novel 1,2,3-Triazole-8-quinolinol Hybrids. ACS Omega, 9(23) (2024), 25395–25409.

[29] Schrödinger Release 2022-4: QikProp. Schrödinger, LLC, New York, NY, USA, (2022).

[30] Gorgun, E., Ali, A., & Islam, M. S. Biocomposites of poly (lactic acid) and microcrystalline cellulose: influence of the coupling agent on thermomechanical and absorption characteristics. ACS Omega, 9(10) (2024), 11523-11533.

[31] Gürdaş Mazlum, S., & Lodos, D. Modelling of Rheological Behaviour of Persimmon Puree. Turkish Journal of Agriculture - Food Science and Technology, 13(2) (2025), 439–445.

[32] Medetalibeyoğlu, H., Atalay, A., Sağlamtaş, R., Manap, S., Ortaakarsu, A. B., Ekinci, E., ... & Tüzün, B. Synthesis, design, and cholinesterase inhibitory activity of novel 1,2,4-triazole Schiff bases: A combined experimental and computational approach. International Journal of Biological Macromolecules, 306 (2025), 141350.

[33] Tüzün, B., Agbektas, T., Naghiyev, F. N., Tas, A., Zontul, C., Ozum, U., ... & Mamedov, I. G. In vitro cytotoxicity, gene expression, bioinformatics, biochemical analysis, and in silico analysis of synthesized carbonitrile derivatives. Monatshefte für Chemie-Chemical Monthly, (2025), 1-22.

[34] Bouabbadi, A., Rbaa, M., Tüzün, B., Hmada, A., Dahmani, K., Kharbouch, O., ... & Harcharras, M. Novel 8-hydroxyquinoline compounds used to inhibit mild steel corrosion in the presence of hydrochloric acid 1.0 M: an experimental and theoretical electrochemical study. Canadian Metallurgical Quarterly, (2025), 1-18.

[35] Schrader, T., Khanifaev, J., & Perlt, E. Koopmans' theorem for acidic protons. Chemical Communications, 59(93) (2023), 13839-13842.

[36] Pearson, R. G. Hard and soft acids and bases. Journal of the American Chemical Society, 85(22) (1963), 3533-3539.

[37] Pearson, R. G. Hard and soft acids and bases. Journal of the American Chemical Society, 85(22) (1963), 3533-3539.

[38] Parr, R. G., & Chattaraj, P. K. Principle of maximum hardness. Journal of the American Chemical Society, 113(5) (1991), 1854-1855.

[39] Ayers, P. W. An elementary derivation of the hard/soft-acid/base principle. The Journal of Chemical Physics, 122(14) (2005).

[40] Phillips, J. C. Generalized Koopmans' Theorem. Physical Review, 123(2) (1961), 420.

[41] Güçlü, G., Tüzün, B., Uçar, E., Eruygur, N., Ataş, M., İnanır, M., ... & Coşge Şenkal, B. Phytochemical and Biological Activity Evaluation of Globularia orientalis L. Korean Journal of Chemical Engineering, (2025), 1-17.

[42] Tüzün, B., Agbektas, T., Naghiyev, F. N., Tas, A., Zontul, C., Ozum, U., ... & Mamedov, I. G. In vitro cytotoxicity, gene expression, bioinformatics, biochemical analysis, and in silico analysis of synthesized carbonitrile derivatives. Monatshefte für Chemie-Chemical Monthly, (2025), 1-22.

[43] Bouabbadi, A., Rbaa, M., Tüzün, B., Hmada, A., Dahmani, K., Kharbouch, O., ... & Harcharras, M. Novel 8-hydroxyquinoline compounds used to inhibit mild steel corrosion in the presence of hydrochloric acid 1.0 M: an experimental and theoretical electrochemical study. Canadian Metallurgical Quarterly, (2025), 1-18.

[44] Maliyakkal, N., Taslimi, P., Tüzün, B., Menadi, S., Cacan, E., Beeran, A. A., ... & Mathew, B. Cholinesterase Inhibition and Anticancer Properties of [4-(Benzyloxy)phenyl]{Methylidene}hydrazinylidene]-1,3-dihydro-2H-Indol-2-ones Using Swiss Target-guided Prediction. Current Computer-Aided Drug Design, (2025).

[45] Cevik, U. A., Ünver, H., Bostancı, H. E., Tüzün, B., Gedik, N. İ., & Kocyigit, Ü. M. New hydrazone derivatives: synthesis, characterization, carbonic anhydrase I-II enzyme inhibition, anticancer activity and in silico studies. Zeitschrift für Naturforschung C, (2025).

[46] Karatas, H., Kul, İ. B., Aydin, M., Tüzün, B., Taslimi, P., & Kokbudak, Z. Alzheimer's Disease Drug Design by Synthesis, Characterization, Enzyme Inhibition, In Silico, SAR Analysis and MM-GBSA Analysis of Schiff Bases Derivatives. Korean Journal of Chemical Engineering, (2025), 1-19.

[47] Tüzün, B. Evaluation of cytotoxicity, chemical composition, antioxidant potential, apoptosis relationship, molecular docking, and MM-GBSA analysis of Rumex crispus leaf extracts. Journal of Molecular Structure, 1323 (2025), 140791.

[48] Akkus, M., Kirici, M., Poustforoosh, A., Erdogan, M. K., Gundogdu, R., Tüzün, B., & Taslimi, P. Phenolic Compounds: Investigating Their Anti-Carbonic Anhydrase, Anti-Cholinesterase, Anticancer, Anticholinergic, and Antiepileptic Properties Through Molecular Docking, MM-GBSA, and Dynamics Analyses. Korean Journal of Chemical Engineering, (2025), 1-20.

[49] Ullah, N., Alam, A., Tüzün, B., Rehman, N. U., Ayaz, M., Elhenawy, A. A., ... & Ahmad, M. Synthesis of novel thiazole derivatives containing 3-methylthiophene carbaldehyde as potent anti α-glucosidase agents: In vitro evaluation, molecular docking, dynamics, MM-GBSA, and DFT studies. Journal of Molecular Structure, 1321 (2025), 140070.

[50] Çiçek, S., Korkmaz, Y. B., Tüzün, B., Işik, S., Yilmaz, M. T., & Özoğul, F. A study on insecticidal activity of the fennel (Foeniculum vulgare) essential oil and its nanoemulsion against stored product pests and molecular docking evaluation. Industrial Crops and Products, 222 (2024), 119859.

[51] Kapancık, S., Çelik, M. S., Demiralp, M., Ünal, K., Çetinkaya, S., & Tüzün, B. Chemical composition, cytotoxicity, and molecular docking analyses of Thuja orientalis extracts. Journal of Molecular Structure, 1318 (2024), 139279.

[52] Manap, S., Medetalibeyoğlu, H., Kılıç, A., Karataş, O. F., Tüzün, B., Alkan, M., ... & Yüksek, H. Synthesis, molecular modeling investigation, molecular dynamic and ADME prediction of some novel Mannich bases derived from 1,2,4-triazole, and

assessment of their anticancer activity. Journal of Biomolecular Structure and Dynamics, 42(21) (2024), 11916-11930.

[53] Myroslava, O., Poustforoosh, A., Inna, B., Parchenko, V., Tüzün, B., & Gutyj, B. Molecular descriptors and in silico studies of 4-((5-(decylthio)-4-methyl-4n-1,2,4-triazol-3-yl)methyl)morpholine as a potential drug for the treatment of fungal pathologies. Computational Biology and Chemistry, 113 (2024), 108206.

[54] Ganbarov, K., Huseynzada, A., Binate, G., Sayin, K., Sadikhova, N., Ismailov, V., ... & Algherbawi, A. Biological and in silico studies of methyl 2-(2-methoxy-2-oxoethyl)-4-methylfuran-3-carboxylate as a promising antimicrobial agent. Acta Scientiarum - Technology, 47(1) (2025).

[55] Prabha, K., Rajendran, S., Gnanamangai, B. M., Sayin, K., Prasad, K. R., & Tüzün, G. Synthesis of novel isostere analogues of naphthyridines using CuI catalyst: DFT computations (FMO, MEP), molecular docking and ADME analysis. Tetrahedron, 168 (2024), 134323.

[56] Huseynzada, A., Mori, M., Meneghetti, F., Israyilova, A., Tüzün, G., Sayin, K., ... & Abbasov, V. Synthesis, crystal structure, Hirshfeld surface, computational and antibacterial studies of a 9-phenanthrenecarboxaldehyde-based thiodihydropyrimidine derivative. Journal of Molecular Structure, 1267 (2022), 133571.

[57] Kafa, A. H. T., Tüzün, G., Güney, E., Aslan, R., Sayın, K., Tüzün, B., & Ataseven, H. Synthesis, computational analyses, antibacterial and antibiofilm properties of nicotinamide derivatives. Structural Chemistry, 33(4) (2022), 1189-1197.

[58] Yildiz, H., Tüzün, G., & Erbayraktar, E. Sarı Kantoron (Hypericum perforatum) Bitkisinin Antioksidan ve Antimikrobiyal Özellikleri Üzerine Bir Araştırma. ISPEC Journal of Science Institute, 1(1) (2022), 27-32.

[59] Lipinski, C. A. Lead-and drug-like compounds: the rule-of-five revolution. Drug Discovery Today: Technologies, 1(4) (2004), 337-341.

[60] Lipinski, C. A., Lombardo, F., Dominy, B. W., & Feeney, P. J. Experimental and computational approaches to estimate solubility and permeability in drug discovery and development settings. Advanced Drug Delivery Reviews, 23 (1997), 3-25.

[61] Jorgensen, W. J., & Duffy, E. M. Prediction of drug solubility from structure. Advanced Drug Delivery Reviews, 54(3) (2002), 355-366.